^{1}H NMR Investigation of the Role of Intrinsic Heme versus Protein-Induced Rhombic Perturbations on the Electronic Structure of Low-Spin Ferrihemoproteins: Effect of Heme Substituents on Heme Orientation in Myoglobin

Urszula Kolczak,[†] Jon B. Hauksson,[†] Nicolette L. Davis,[†] Usha Pande,[†] Jeffrey S. de Ropp,[‡] Kevin C. Langry,[†] Kevin M. Smith,[†] and Gerd N. La Mar*[,†]

Contribution from the Department of Chemistry and NMR Facility, University of California, Davis, California 95616

Received August 24, 1998. Revised Manuscript Received December 2, 1998

Abstract: Solution ^{1}H NMR spectroscopy has been used to characterize the cyanomet myoglobin complexes of a variety of chemically modified hemins in order to elucidate the importance of hemin peripheral electronic, relative to axial His imidazole-induced, rhombic perturbations in raising the orbital degeneracy of the π-bonding d_{xz},d_{yz} orbitals. Variation of the hemin 2- and/or 4-position substituents among hydrogen, ethyl, vinyl, acetyl, and formyl groups leads to conserved molecular structure of the heme pocket and orientation of the major magnetic axis for the heme iron, but systematically perturbed heme methyl contact shift patterns. Two strongly rhombically perturbed hemins with single acetyl groups on either pyrrole I or II exhibit heme methyl contact shift patterns and characteristic deviations from Curie law that are very similar to that induced in pseudosymmetric hemins upon incorporation into metMbCN in the alternate orientations about the α,γ-meso axis. The perturbation due to the 4-acetyl group and the axial His bond leads to increased contact shift spread and stronger deviations from Curie behavior compared to WT, indicative of an increased d_{xz}/d_{yz} spacing relative to WT. In contrast, the perturbation due to the 2-acetyl group and axial His nearly cancel, leading to a highly compressed methyl contact shift spread and weaker deviations from Curie behavior than WT. It is shown, moreover, that the larger d_{xz}/d_{yz} splitting with 4-acetylhemin, and the smaller splitting with 2-acetylhemin, relative to WT, result in the expected increase and decrease, respectively, for the axial His contact shift relative to WT. Comparison of the methyl shifts for 16 peripherally modified hemins as model compounds and incorporated into metMbCN shows that the rhombic influences are additive in each of the complexes. Thus, the present results show that chemical functionality of the heme periphery contributes to raising the orbital degeneracy of the heme iron and that such influences can account for orbital ground states that are not necessarily aligned with the axial His orientation. The range of variant 2- and/or 4-substitutions have led to equilibrium heme orientations that are largely the same as found in WT Mb, except for a 4-ethyl group, which favors the reversed heme orientation by 2:1.

Introduction

The hyperfine shift pattern for low-spin hemins is characterized by the dominant contact shifts which, in approximate 4-fold symmetry outside a protein matrix, exhibit[1,2] comparable contact shifts for the four methyl groups at positions 1, 3, 5, and 8 (labeling in Figure 1). Upon incorporation of a hemin into the asymmetric protein environment of a low-spin cyanide-ligated ferrimyoglobin, metMbCN,[3] the approximate in-plane, 4-fold symmetry is lifted, with the dominant contribution to the protein-induced rhombic perturbation proposed to arise from the π bonding between the hemin iron and the axial His F8 imidazole ring.[4−6] The particular pattern of the hemin methyl contact shifts thus depends on the orientation of the axial His imidazole plane relative to the hemin.[4−7] Alignment of the imidazole plane with a N−Fe−N vector leads to an orbital ground state which allows π delocalization only into pyrroles whose N−Fe−N axis is normal to the imidazole plane.[6] Thus, in the case of sperm whale Mb, where the His F8 plane is nearly coincident with the N_{II}−Fe−N_{IV} vector[8] in the crystallographic orientation of the hemin (A in Figure 1), the resulting $(d_{xy})^2(d_{xz})^2d_{yz}$ ground state leads to large contact shifts for 1-CH_3, 5-CH_3 and small contact shifts[4] for 3-CH_3, 8-CH_3. Even early considerations[9] recognized that

* Corresponding author: (phone) (530) 752-0958; (e-mail) lamar@indigo.ucdavis.edu.

† Department of Chemistry.

‡ NMR Facility.

(1) Cavaleiro, J. A. S.; Rocha Gonsalves, A. M. d'A.; Kenner, G. W.; Smith, K. M.; Shulman, R. G.; Meyer, A.; Yamane, T. *J. Chem. Soc. Chem. Commun*. **1974**, 393−393.

(2) La Mar, G. N.; Viscio, D. B.; Smith, K. M.; Caughey, W. S.; Smith, M. L. *J. Am. Chem. Soc*. **1978**, *100*, 8085−8092. Davis, N. L. Ph.D. Dissertation, University of California, Davis, 1982.

(3) Abbreviations used: Mb, myoglobin; MbCN, ferric myoglobin cyanide; NOESY, 2D nuclear Overhauser spectroscopy; TOCSY, 2D total correlation spectroscopy; DSS, 2,2′-dimethyl-2-silapentane-5-sulfonate.

(4) Mayer, A.; Ogawa, S.; Shulman, R. G.; Yamane, T.; Cavaleiro, J. A. S.; Rocha Gonsalves, A. M. d'A.; Kenner, G. W.; Smith, K. M. *J. Mol. Biol.* **1974**, *86*, 740−756.

(5) Shulman, R. G.; Glarum, S. H.; Karplus, M. *J. Mol. Biol.* **1971**, *57*, 93−115.

(6) Traylor, T. C.; Berzinis, A. P. *J. Am. Chem. Soc.* **1980**, *102*, 2844−2840.

(7) Satterlee, J. D. *Annu. Rep. NMR Spectrosc*. **1986**, *77*, 79−178. Bertini, I.; Turano, P.; Vila, A. J. *Chem. Rev*. **1993**, *93*, 2833−2932. Yamamoto, Y. *Annu. Rep. NMR Spectrosc*. **1998**, *36*, 1−77.

(8) Kuriyan, J.; Wilz, S.; Karplus, M.; Petsko, G. A. *J. Mol. Biol*. **1986**, *192*, 133−154.

(9) Horrocks, W. DeW., Jr.; Greenberg, E. S. *Biochim. Biophys. Acta* **1973**, *322*, 38−44

10.1021/ja983045x CCC: $18.00
Published on Web 01/20/1999

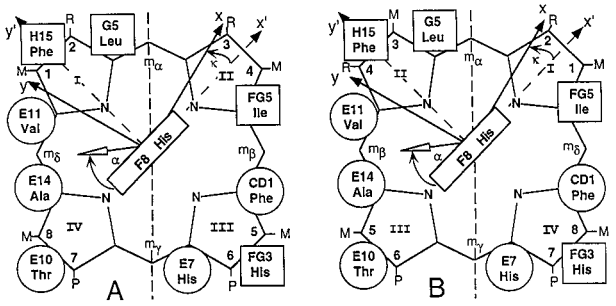

Figure 1. 2R,4R′-Hemin in the heme pocket as found in sperm whale Mb (A) and when rotated by 180° about the α,γ-meso axis (B). The expected dipolar shifted residues in the heme pocket and their heme contact positions are identified by the helical (i.e., E7) or loop (FG3) positions, with proximal and distal residues indicated by squares and circles, respectively. The heme is labeled in the Fisher notation. *x*′, *y*′, *z*′ is a pseudosymmetric, iron-centered coordinate system defined by the crystal structure of MbCO, and *x*, *y*, *z* represents the magnetic coordinate system where the paramagentic susceptibility tensor, χ, is diagonal. The two coordinate systems are related by the Euler rotation $\Gamma(\alpha,\beta,\gamma)$, where $(x,y,z) = (x',y',z')\Gamma(\alpha,\beta,\gamma)$, with β the tilt of the major magnetic axis from the heme normal, α the direction of tilt, as given by the projection of the *z* axis on the heme plane and the *x*′ axis, and $\kappa \sim \alpha + \gamma$ represents the orientation of the rhombic axes projected on the heme plane. It is noted that this reference coordinate system is rotated by 45° relative to that used previously[20,21] and α is referenced to the $+x'$ rather than $-x'$ axis; this leaves β unchanged, but α(new) = α(old) + 135) and κ(new) = κ(old) − 45°.

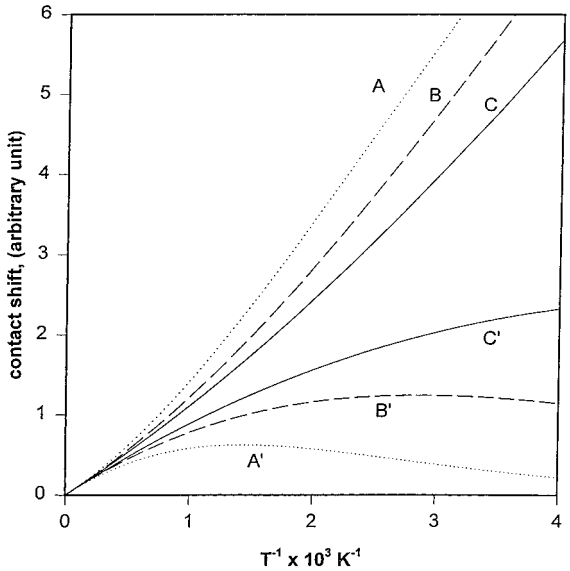

Figure 2. Simulations of the predicted temperature dependence for the heme methyls for the case of a $(d_{xy})^2(d_{xz})^2(d_{yz})$ orbital ground state that delocalizes spin density only into pyrroles I and III, with resulting identical contact shifts for 1-CH_3, 5-CH_3 (A, B, C); zero contact shifts for 3-CH_3, 8-CH_3 (A′, B′, C′), and thermal population of a $(d_{xy})^2(d_{xz})$-$(d_{yz})^2$ excited orbital state that reverses the environment of the 1-CH_3, 5-CH_3 and 3-CH_3, 8-CH_3 groups, for an energy spacing of (A, A′) 150, (B, B′) 300, and (C, C′) 600 cm^{-1}.

the raising of the orbital degeneracy by the protein was likely to be comparable to kT. Thus, the hemin methyl contact shift pattern should reflect some thermal averaging of the excited doublet, $(d_{xy})^2(d_{xz})(d_{yz})^2$, for which the orbital hole, and hence hemin methyl contact shift pattern, are reversed (i.e., large 3-CH_3, 8-CH_3 and small 1-CH_3, 5-CH_3 contact shifts) for hemin orientation as in Figure 1A. A schematic representation of what may be expected in the simplistic picture of an imidazole aligned precisely along the $N_{II}-Fe-N_{III}$ vector, strict T^{-1} dependence (with zero intercept) for shifts for a given orbital state, and negligible dipolar shifts (see below) is illustrated in Figure 2 for different spacing between the d_{xz} and d_{yz} orbitals. In fact, all cyanometglobins for which the complete hemin methyl assignments are available over a range of temperature exhibit the anomalous temperature behavior,[10−16] and analysis of some of these data been proposed to provide the spacing of the two relevant orbital states.[17] A similar phenomenon is observed in ferricytochromes.[18,19]

There are several indications that there are contributions other than the axial His to the rhombic perturbations in globins. First, the rotational positions of the axial His[8] and rhombic axes[20−22] do not conform quantitatively to the counterrotation rule[23,24] for these two angles. Second, two proteins with very similar His orientation relative to the hemin, sperm whale Mb[8] and human Hb,[25] exhibit some key differences in contact shift pattern and temperature behavior.[4,11,16] Last, and more directly, it has been observed that asymmetrical mesosubstitution in low-spin, ferric tetraarylporphyrins leads to contact shift asymmetry and deviations from Curie law indicative of resolution of the orbital degeneracy.[26] One possible such rhombic perturbation in native protohemin, though likely less important than the axial His,[27] is that due to the direct electronic influence of the 2,4-vinyl groups, whose influence, moreover, can be modulated by differential protein-induced vinyl/heme coplanarity. A low-symmetry perturbation of vinyl groups on hemin, compared to the essentially 4-fold symmetric hemin, is evident in that the four methyl groups can exhibit significant contact shift differences even outside the protein matrix.[1,2,28]

(10) Wüthrich, K.; Shulman, R. G.; Peisach, J. *Proc. Natl. Acad. Sci. U.S.A.* **1968**, *60*, 373−380.
(11) La Mar, G. N.; Emerson, S. D.; Lecomte, J. T. J.; Pande, U.; Smith, K. M.; Craig, G. W.; Kehres, L. A. *J. Am. Chem. Soc.* **1986**, *108*, 5568−5573.
(12) Peyton, D. H.; La Mar, G. N.; Pande, U.; Ascoli, F.; Smith, K. M.; Pandey, R. K.; Parish, D. W.; Bolognesi, M.; Brunori, M. *Biochemistry* **1989**, *28*, 4880−4887.
(13) Wu, Y.; Chien, E. Y. T.; Sligar, S. G.; La Mar, G. N. *Biochemistry* **1998**, *37*, 6979−6990.
(14) Yamamoto, Y.; Suzuki, T. Biochim. Biophys. Acta **1993**, *1163*, 284−296. Yamamoto, Y.; Iwafume, K.; Nanai, N.; Ogawa, A.; Chujo, R.; Suzuki, T. *Eur. J. Biochem.* **1991**, *198*, 299−306.
(15) Alam, S. L.; Satterlee, J. D. *Biochemistry* **1994**, *33*, 4008−4018.
(16) Kolczak, U.; Han, C.; Sylvia, L. A.; La Mar, G. N. *J. Am. Chem. Soc.* **1997**, *119*, 12643−12654
(17) Shokhirev, N. V.; Walker, F. A. *J. Phys. Chem.* **1995**, *99*, 17795−17804.
(18) Keller, R. M.; Wüthrich, K. *Biochim. Biophys. Acta* **1972**, *285*, 326−336. McDonald, C. C.; Phillips, W. D. *Biochemistry* **1973**, *12*, 3170−3186. Smith, G. M. *Biochemistry* **1979**, *18*, 1628−1634. Senn, H.; Wüthrich, K. *Biochim. Biophys. Acta* **1983**, *743*, 69−81. Timkovich, R.; Cork, M. S.; Taylor, P. V. *Biochemistry* **1984**, *23*, 3521−3533. Turner, D. L. *Eur. J. Biochem.* **1993**, *211*, 563−568. Turner, D. L. *Eur. J. Biochem.* **1995**, *227*, 829−837.
(19) Brennan, L.; Turner, D. L. *Biochim. Biophys. Acta* **1997**, *1342*, 1−12. Banci, L.; Bertini, I.; Luchinat, C.; Pierattelli, R.; Shokhirev, N. V.; Walker, F. A. *J. Am. Chem. Soc.* **1998**, *120*, 8472−8479.
(20) Emerson, S. D.; La Mar, G. N. *Biochemistry* **1990**, *29*, 1556−1566.
(21) Rajarathnam, K.; La Mar, G. N.; Chiu, M. L.; Sligar, S. G. *J. Am. Chem. Soc.* **1992**, *114*, 9048−9058.
(22) Nguyen, B. D.; Xia, Z.; Yeh, D. C.; Vyas, K.; Deaguero, H.; La Mar, G. N. *J. Am. Chem. Soc.*, in press.
(23) (a) Oosterhuis, W. T.; Lang, G. *Phys. Rev.* **1969**, *178*, 439−456. (b) Byrn, M. P.; Katz, B. A.; Keder, N. L.; Levan, K. R.; Magurany, C. J.; Miller, K. M.; Pruitt, J. W.; Strouse, C. E. *J. Am. Chem. Soc.* **1983**, *105*, 4916−4922.
(24) Shokhirev, N. A.; Walker, F. A. *J. Am. Chem. Soc.* **1998**, *120*, 981−990.
(25) Baldwin, J. M. *J. Mol. Biol.* **1980**, *136*, 103−128.
(26) Walker, F. A.; Simonis, U. *Biol. Magn. Reson.* **1993**, *12*, 133−274 and references therein.
(27) Banci, L.; Pierattelli, R.; Turner, D. L. *Eur. J. Biochem.* **1995**, *232*, 522−527.

Our interest in this report is to establish how heme peripheral substituents contribute to the rhombic environment of a hemin in a low-spin, ferric hemoprotein using a variety of 2- and/or 4-position substituents (see Figure 1), including hydrogen (H), methyl (M), ethyl (E), vinyl (V), acetyl (A), and formyl (F) groups. Of particular interest are the two hemins with 2R = H, 4R′ = A and 2R = A, 4R′ = H, each of which exhibit strong rhombic electronic perturbations on a single pyrrole. The methyl peaks in the ^{1}H NMR spectra of the biscyano 2R,4R′-hemin complexes have been assigned.[2,28] The substituent electronic influence leads to as small a spread of hemin methyl signals as ~0.4 ppm for the nearly 4-fold symmetric 2R = 4R′ = E or 2R = 4R′ = M and to as large[28] a spread as 22 ppm for 2R = A, 4R′ = H. The questions we seek to address herein are, Do the hemin peripheral substituents contribute to the magnitude of the spacing between the two orbital states $(d_{xy})^2(d_{xz})^2(d_{yz})$ and $(d_{xy})^2(d_{yz})^2(d_{xz})$, and, by inference, contribute to the orientation of the orbital ground state?. And, is there a predictable relationship between the hemin methyl hyperfine shifts for a model and those when it is incorporated into a low-spin ferrihemoprotein? Last, the hemin orientation in globins is determined by subtle hemin−protein contacts that differentiate the asymmetric placement of the 2-vinyl and 4-vinyl groups on pyrroles I and II, with mammalian globins[8,25,29,30] generally favoring hemin orientation A in Figure 1, but with other species,[31] and in particular invertebrates[12,32] exhibiting much less preference. The present permutation of 2,4-substituents provides an opportunity to monitor their influence on the stability of the alternate hemin orientations.

Experimental Section

Sample Preparation. Sperm whale Mb was purchsed from Sigma Chemical Co. Apo Mb was prepared by standard methods,[33] and the various hemes were reconstituted as described in detail previously.[34,35] Protein samples were exchanged into ^2H_2O using an Amicon ultrafiltration device. Twelve chemically modified hemins are used with different substituents at positions 2 and 4 and are referred to as 2R,-4R′-hemin. These include 2R = 4R′ = E (also known as mesohemin); 2R = 4R′ = H (also known as deuterohemin); 2R = H, 4R′ = V (vinyl) (also known as pemptohemin); and its 3-methyl deuterated derivative; 2R = V, 4R′ = H (also known as isopemptohemin) and its 1-methyl deuterated derivative; 2R = 4R′ = A (acetyl) and its 1,3-methyl deuterated derivative; 2R = H, 4R′ = A and its 3-methyl deuterated derivative; 2R = A, 4R = H, and its 1-methyl deuterated derivative; 2R = F, 4R′ = V (formyl) (also known as *spirographis* hemin); 2R = V, 4R′ = F (also known as *isospirographis* hemin); 2R = E, 4R = H; 2R = H, 4R′ = E; 2H,4E-hemin and its 3-methyl deuterated derivative, 2R = E, 4R = H and its 1-methyl deuterated derivative, and 2R = 4R′ = M (methyl), each of whose syntheses have been reported previously.[36,37]

NMR Spectra. ^{1}H NMR spectra were collected on Nicolet NT500 and GE Ω-500 NMR spectrometers operating at 500 MHz. The chemical shifts were referenced to 2,2′-dimethyl-2-silapentane-5-sulfonate (DSS) through the water peak. The 1D experiments, nonselective T_1's, WEFT spectra,[38] and steady-state NOEs were carried out as described previously.[39] The 1D data were processed on a Sun workstation using GE UNIX Ω software; 500-MHz 2D NOESY[40,41] and TOCSY[42] were collected by using 2048 points for t_2, 512 blocks for t_1, typically 256 scans for each block, and a repetition rate ~2 s^{-1}. The spectral window was varied from 10 to 30 kHz, and the mixing times were 50 ms for NOESY and 30 ms for TOCSY. The 2D data were processed on the Silicon Graphics (SGI) workstation using the softare package Felix from Biosym (San Diego) and consisted of 20−40°-shifted sine-bell-squared apodization in both dimensions, phase corrected and baseline straightened in both dimensions.

Magnetic Axes Determination. The magnetic axes were determined as described in detail previously.[20−22,43] Experimental dipolar shifts, δ_{dip}(obs), for structurally conserved portions of the heme pocket, relative to MbCO,[8] were used as input to search for the Euler rotation, Γ(α,β,γ), that transforms the molecular pseudosymmetry coordinates (x', y', z' or r, θ', Ω' (Figure 1)), readily obtained from crystal coordinates,[8] into magnetic axes,[43] x, y, z or R, θ, Ω, i.e., $(x, y, z) = (x',y',z')\Gamma(\alpha,\beta,\gamma)$, by minimizing the following global error function:

$$F/n = \sum|\delta_{dip}(\text{obs}) - \delta_{dip}(\text{calc})|^2 \quad (1)$$

where

$$\delta_{dip}(\text{calc}) = \frac{\mu_o}{12\pi}[\Delta\chi_{ax}(3\cos^2\theta' - 1)R^{-3} + 3/2\Delta\chi_{rh}(\sin^2\theta'\cos 2\Omega')R^{-3}]\Gamma(\alpha,\beta,\gamma) \quad (2)$$

where μ_o is the permutability of vacuum, $\Delta\chi_{ax} = \chi_{zz} - 1/2(\chi_{xx} + \chi_{yy})$, $\Delta\chi_{rh} = \chi_{xx} - \chi_{yy}$, with χ_{ii} ($i = x, y, z$) the components of the diagonal paramagnetic susceptibility tensor, and

$$\delta_{dip}(\text{obs}) = \delta_{DSS}(\text{obs}) - \delta_{DSS}(\text{dia}) \quad (3)$$

where δ_{DSS}(obs) is the observed chemical shift referenced to DSS. δ_{DSS}-(dia) is the shift in the isostructural diamagnetic MbCO complex[44] or calculated for protons whose δ_{DSS}(dia) are not available by using δ_{DSS}-(dia) = $\delta_{tetr} + \delta_{sec} + \delta_{rc}$, where δ_{tetr} is the shift in an unfolded tetra peptide,[45] δ_{sec} is the shift of an amino acid proton typical for α-helices, β-strand, coils, etc.,[46] and δ_{rc} is the heme-induced ring current shift.[47] Minimizing the error function, F/n, in eq 1 was performed over three parameters, α, β, γ, using available[22] $\Delta\chi_{ax} = 2.48 \times 10^{-8}$ m^3/mol and

(28) La Mar, G. N.; Budd, D. L.; Viscio, D. B.; Smith, K. M.; Langry, K. C. *Proc. Natl. Acad. Sci. U.S.A.* **1978**, *75*, 5755−5759.
(29) La Mar, G. N.; Davis, N. L.; Parish, D. W.; Smith, K. M. *J. Mol. Biol.* **1983**, *168*, 887−896. Lecomte, J. T. J.; Johnson, R. D.; La Mar, G. N. *Biochim. Biophys. Acta* **1985**, *829*, 268−274.
(30) La Mar, G. N.; Yamamoto, Y.; Jue, T.; Smith, K. M.; Pandey, R. K. *Biochemistry* **1985**, *24*, 3826−3831.
(31) Levy, M. J.; La Mar, G. N.; Jue, T.; Smith, K. M.; Pandey, R. K.; Smith, W. S.; Livingston, D. J.; Brown, W. D. *J. Biol. Chem.* **1985**, *260*, 13694−13698.
(32) La Mar, G. N.; Smith, K. M.; Gersonde, K.; Sick, H.; Overkamp, M. *J. Biol. Chem.* **1980**, *255*, 66−70. Peyton, D. H.; La Mar, G. N. Gersonde, K. *Biochim. Biophys. Acta* **1988**, *954*, 82−94.
(33) Teale, F. W. J. *Biochim. Biophys. Acta* **1959**, *35*, 543.
(34) Antonini, E.; Burnori, M.; Caputo, A.; Chiancone, E.; Rossi-Fanelli, A.; Wyman, J. *Biochim. Biophys. Acta* **1964**, *79*, 284−292.
(35) La Mar, G. N.; Toi, H.; Krishnamoorthi, R. *J. Am. Chem. Soc.* **1984**, *106*, 6395−6401.
(36) Smith, K. M.; Eivazi, F.; Langry, K. C.; Almeida, J. A. P. B.; Kenner, G. W. *Bioorg. Chem.* **1979**, *8*, 485−495.
(37) La Mar, G. N.; de Ropp, J. S.; Smith, K. M.; Langry, K. C. *J. Am. Chem. Soc.* **1983**, *105*, 4576−4580.
(38) Gupta, R. K. *J. Magn. Reson.* **1976**, *24*, 461−465.
(39) Emerson, S. D.; Le Mar, G. N. *Biochemistry* **1990**, *29*, 1546−1556.
(40) Jeener, J.; Meier, B. H.; Bachmann, P.; Ernst, R. R. *J. Chem. Phys.* **1979**, *71*, 4546−4553.
(41) States, D. J.; Haberkorn, R.; Ruben, D. *J. Magn. Reson.* **1982**, *48*, 286−296.
(42) Griesinger, C.; Otting, G.; Wütrich, K.; Ernst, R. R. *J. Am. Chem. Soc.* **1988**, *110*, 7870−7872.
(43) The reference coordinate system used previously[10,14,20,25,26] has been redefined to bring it into conformity with that used elsewhere, with the x', y' axes passing through the pyrrole N−Fe−N rather than the meso-Fe-meso axis; moreover, α is defined as the angle between the projection of the z axis on the $x'y'$ plane and the x' rather than the $-x'$ axis. The definition of β is unchanged, but leads to α(new) = α(old) + 135°, κ(new) = κ(old) −45°.
(44) Mabbutt, B. C.; Wright, P. E. *Biochim. Biophys. Acta* **1985**, *832*, 175−185. Dalvit, C.; Wright, P. E. *J. Mol. Biol.* **1987**, *194*, 313−327. Theriault, Y.; Pochapsky, T. C.; Dalvit, C.; Chiu, M. L.; Sligar, S. G.; Wright, P. E. *J. Biomol. NMR* **1994**, *4*, 491−504.
(45) Bundi, A.; Wüthrich, K. *Biopolymers* **1979**, *18*, 285−297.
(46) Wishart, D. S.; Sykes, B. D.; Richards, F. *J. Mol. Biol.* **1991**, *222*, 311−333.
(47) Cross, K. J.; Wright, P. E. *J. Magn. Reson.* **1985**, *64*, 240−231.

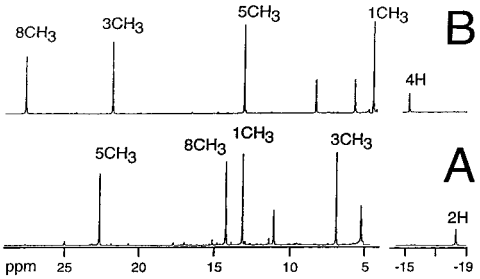

Figure 3. Low-field and high-field portions of the 500 MHz ^{1}H NMR spectra of low-spin, S = 1/2,: (A) bis-cyano 2H,4A-hemin; and (B) bis-cyano 2A,4H-hemin in $C^2H_3O^2H$ at 25 °C, with methyl assignments.[28]

$\Delta\chi_{rh} = -0.58 \times 10^{-8}$ m^3/mol for WT metMbCN,[22,48] as described in detail previously.[20−22] For the iron ligands, the hyperfine shifts, δ_{hf}, is obtained through:

$$\delta_{hf}(\text{obs}) = \delta_{DSS}(\text{obs}) - \delta_{DSS}(\text{dia}) \quad (4)$$

and this can be further factored into the contact and dipolar contribution:

$$\delta_{hf} = \delta_{dip} + \delta_{con} \quad (5)$$

Results

NMR Spectra for Biscyano 2H,4A-hemin and 2A,4H-hemin. These two hemins serve as unique probes of peripheral perturbation because they possess a single substitution (the acetyl group) with electronic properties very different from that of any other substituent on the hemin. The acetyl group can be introduced into either pyrrole I (2A,4H-hemin) or II (2H,4A-hemin), imparting a large and clearly "localized" rhombic perturbation to the unpaired spin distribution. The ^{1}H NMR spectra for the two model complexes in $C^2H_3O^2H$ are shown in Figure 3, together with the previously reported assignments.[28] The effect of temperature on the heme methyl hyperfine shifts, in the form of Curie plots, is shown in Figure 4A and C. In contrast to all other model compounds[49] without A or F substituents, the four methyls exhibit very different slopes in the Curie plot, with the highest field methyl in each case exhibiting strong anti-Curie behavior. In fact, 2H,4A-hemin-$(CN)_2^-$ exhibits (Figure 3A) a methyl contact shift pattern (5-CH_3 > 8-CH_3 ≳ 1-CH_3 > 3-CH_3) and methyl shift spread similar to that observed for a nominally symmetric hemin incorporated into metMbCN[4,11,28] in the orientation in Figure 1A. Thus the 4-acetyl group is as effective in raising the orbital degeneracy outside the protein matrix as is the axial His in raising the orbital degeneracy of a more 4-fold symmetric hemin in the pocket of metMbCN.

In contrast, 2A,4H-hemin$(CN)_2^-$ exhibits (Figure 3B) the methyl contact shift pattern, 8-CH_3 > 3-CH_3 > 5-CH_3 > 1-CH_3, that is the same as exhibited by a nominally symmetric hemin upon incorporation into metMbCN with the *reversed heme orientation* [28,29] *as in Figure 1B*. Thus, an electronic perturbation of the hemin by peripheral functional groups manifests itself in the ^{1}H NMR spectral parameters (shift pattern, Curie slopes) of the low-spin, biscyano hemin models in essentially the same fashion as do protein-induced rhombic perturbations due to the axial His bond upon incorporation into metMbCN.

(48) These are standard SI units, as also used in ref 22. The anisotropies in ref 20 must be multiplied by 4π; those in ref 21 must be multiplied by $12\pi N_A$ for $\Delta\chi_{ax}$ and $-8\pi N_A$ for $\Delta\chi_{rh}$.

(49) Viscio, D. B.; La Mar, G. N. *J. Am. Chem. Soc.* **1978**, *100*, 8092−8096.

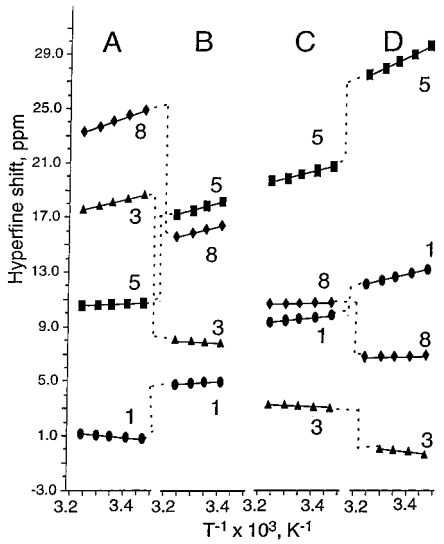

Figure 4. Curie plot (chemical shift versus reciprocal absolute temperature) for (A) biscyano complex of 2A,4H-hemin in $C^2H_3O^2H$, (B) 2A,4H-metMbCN in ^2H_2O, (C) biscyano complex of 2H,4A-hemin in $C^2H_3O^2H$, and (D) 2H,4A-metMbCN in ^2H_2O. Assignments are 1-CH_3 (circle), 3-CH_3, (triangle), 5-CH_3 (square), and 8-CH_3 (diamond).

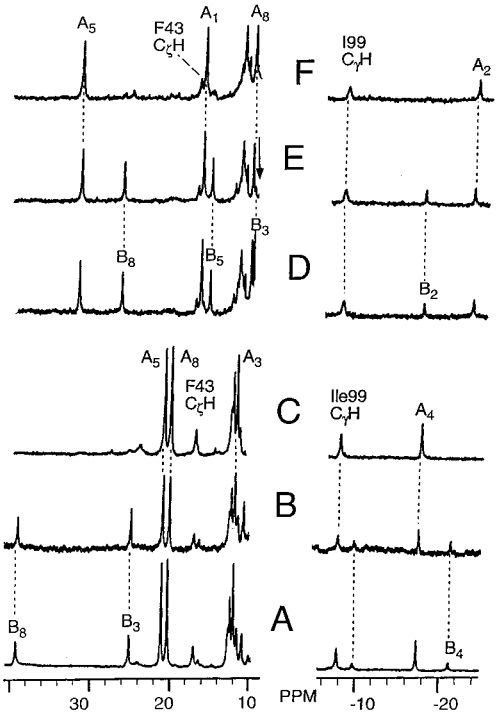

Figure 5. Resolved portions of the 500-MHz ^{1}H NMR spectra of 2A,-4H-metMbCN in ^2H_2O, 0.2 M NaCl, pH 8.6, at 30 °C: (A) immediately after reconstitution when the two heme orientations are comparably populated; (B) immediately after reconstitution with the 3-methyl group perdeuterated; and (C) at equilibrium where the major or "A" orientation predominates by ∼20:1. Resolved portions of the 500-MHz ^{1}H NMR spectra of 2H,4A-metMbCN in ^2H_2O, 0.2 M NaCl, pH 8.6 at 30 °C; (D) immediately after reconstitution when the two heme orientations are comparably populated; (E) immediately after reconstitution with the 1-methyl group perdeuterated; and (F) at equilibrium when the major or "A" orientation predominates. The positions of deuteration are shown by vertical arrows, and peaks are labeled A_i, B_i for the heme orientation as in Figure 1A and B, respectively, with i reflecting the heme position of the methyl (low field) or pyrrole-H (upfield) peaks.

Reconstitution with Isotope-Labeled Hemins. The ^{1}H NMR spectra of 2A,4H-metMbCN (Figure 5A) and 2H,4A -metMbCN (Figure 5D) immediately after reconstitution,[28,35] in the presence

Table 1. Chemical Shifts for Selected Heme and Amino Acid Protons in 2R,4R′-MetMbCN Complexes[a]

2R[b]	4R′[b]	heme[c] orientation	1-CH_3	3-CH_3	5-CH_3	8-CH_3	2H/2CH_3	4H/4CH_3	I99 C_γH	F43 C_ζH	K_{eq}[d]
M	M	A	21.81	6.29	24.80	11.89	18.96	9.68	9.2	17.7	
V	V	A	18.6 (18.2)[e]	4.8 (4.3)	27.1 (25.7)	12.9 (13.1)			−9.6	17.3	0.05
		B	*f* (6.1)	17.7 (17.0)	12.9 (12.8)	27.3 (26.0)			−9.1	17.7	
H	H	A	18.2 (18.9)	6.6 (5.4)	24.4 (25.7)	12.5 (14.1)	−21.0	−15.2	−7.9	16.3	0.05
		B	*f* (6.81)	18.4 (18.0)	12.3 (12.8)	28.9 (27.0)	−13.5	−21.4	−8.9	17.1	
E	E	A	22.0 (21.6)	*f* (5.8)	25.3 (24.7)	13.0 (11.8)			−8.7	16.8	0.10
		B	*f* (9.4)	20.0 (18.5)	11.8 (11.8)	25.6 (24.7)			−7.0	16.3	
A	A	A	11.6 (9.7)	*f* (1.3)	26.8 (25.6)	16.4 (17.0)			−8.2	17.6	0.04
		B	*f* (−2.57)	14.8 (14.0)	11.4 (12.7)	35.9 (29.9)			−8.4	16.0	
H	V	A	18.6 (20.1)	*f* (2.9)	26.4 (26.0)	13.1 (13.4)	−19.6		−9.3	16.6	0.10
		B	*f* (8.0)	17.5 (15.6)	12.2 (13.1)	27.6 (26.3)	−13.0		−8.9	?	
V	H	A	17.8 (17.1)	*f* (6.4)	24.8 (24.7)	12.6 (14.8)		−13.9	−8.1	16.7	0.02
		B	*f* (5.0)	18.0 (19.1)	11.6 (11.8)	28.5 (27.7)		−21.0	−9.2		
H	E	A	18.7 (19.7)	7.3	23.7 (23.6)	14.4 (13.9)	−19.50		−8.0	16.2	1.6
		B	*f* (7.6)	21.2 (20.0)	10.7 (10.7)	28.1 (26.8)	−12.27		−8.4	15.5	
E	H	A	21.7 (21.6)	(4.2)	26.0 (25.5)	12.6 (12.1)		−13.6	−8.6	16.5	∼0.02
		B	*g* (9.5)	*g* (16.9)	*g* (12.6)	*g* (25.0)					
H	A	A	16.3 (19.1)	3.7 (−2.9)	31.0 (30.9)	10.4 (9.3)	−23.3		−7.8	16.9	0.05
		B	*f* (6.9)	10.2 (9.8)	15.8 (18.0)	26.0 (22.2)	−16.6		−7.8	?	
A	H	A	8.6 (9.9)	11.7 (12.3)	20.4 (21.2)	19.7 (23.0)		−17.4	−7.8	16.5	0.05
		B	*f* (−2.2)	24.1 (25.0)	*f* (8.3)	37.8 (35.9)		−21.6	−9.8	16.0	
V	F	A	14.2 (16.1)	*f* (−2.7)	32.4 (31.3)	10.4 (9.8)			−9.0	16.6	0.05
		B	*f* (3.9)	*f* (9.9)	16.4 (18.4)	27.4 (22.7)			−8.0	18.2	
F	V	A	11.1 (11.2)	10.1 (9.9)	22.2 (22.7)	22.0 (22.4)			−8.8	16.4	0.05
		B	*f* (−0.9)	24.2 (22.6)	*f* (9.8)	38.2 (35.3)			−9.6	18.4	

[a] Observed shift in ppm, referenced against DDS, in ^2H_2O, 0.2 M NaCl, pH 8.3 at 25 °C. [b] Substituents at positions 2 and 4; M = methyl; V = vinyl; H = hydrogen; E = ethyl; A = acetyl; F = formyl. [c] Heme orientations A (as in Figure 1A) and B (as in Figure 1B). [d] Equilibrium constant for the relative stabilities of the X-ray heme orientation (Figure 1A) and 180° reversed orientation as in Figure 1B, with K_{eq} = [B]/[A]. [e] Predicted shifts, obtained via eqs 6 and 7, in ppm referenced against DSS, are given in parentheses. [f] Not resolved, and hence not assigned. [g] The 2E,4H-metMbCN was investigated only after equilibrium was reached.

of cyanide, reveals two sets of signals, labeled A_i, B_i ($i = 1-8$) for the A and B hemin orientations (Figure 1), respectively, of which one set (B_i) essentially disappears over time, as shown in the respective NMR spectra at equilibrium (Figure 5C, F). Spectra immediately after reconstitution with 1-C^2H_3-2A,4H-hemin (Figure 5B) and 3-C^2H_3-2H,4A-hemin (Figure 5E) identify the 3-CH_3 peak in the "transient" isomer for the latter and show that none of the resolved methyls for either hemin orientation is due to 1-CH_3 in the former.

In a similar fashion, one or more methyls could be identified unambiguously in both the "transient" and equilibrium species for all but two of the hemins of interest, 2F,4V- and 2V,4F-hemins (see below). In the case of 2A,4A-metMbCN, isotope labeling identified all resolved peaks (not shown; see Supporting Information). In each of the ^{1}H NMR spectra, it was possible to locate the resolved, low-field heme methyls solely by intensity, while the pyrrole-H peaks appear in the characteristic upfield spectral window.[35] The chemical shifts for the obvious hemin methyls and pyrrole-H signals, as well as the highly characteristic resolved low-field,[39,50] strongly relaxed (T_1 ∼20 ms) Phe43(CD1) C_ζH and upfield[39] relaxed (T_1 ∼60 ms) Ile99(FG5) C_γH are listed in Table 1. Following the relative peak intensities of a methyl for each isomer after reconstitution until equilibrium is reached (less than 1 h to several days)[11,28−31] allowed determination of the equilibrium constant for hemin orientational disorder, K_{eq}; the values are included in Table 1.

2D Assignment of 2A,4H- and 2H,4A-metMbCN. The complete heme, axial His, and strongly dipolar shifted residue signals are assigned for the equilibrium heme orientation for these two complexes, as described in detail previously for similar metMbCN complexes[21,22,39,50−52] (relevant 2D data are given in Supporting Information). The heme could be assigned by the standard dipolar connectivity among pyrrole substituents.[50] The proximal His signals are assigned on the basis of the characteristically broad and relaxed (T_1 ∼3 ms) ring C_ϵH and C_δH and the low-field and partially resolved C_βH which, via TOCSY, locates the $C_\beta H_2-C_\alpha$H fragment.[51] The distal residues, Phe43(CD1), Phe33(B14), His64(E7), Val68(E11), and Ala71(E14), in both complexes exhibit the same intraresidue TOCSY and interresidues and heme−residue dipolar contacts as observed in WT.[39] The proximal residues Ala90(F5), Ala94(F9), and C_αH of Leu89(F4) are assigned on the basis of completely conserved contacts to His93(F8) relative to WT. Last, the same contacts between His97(FG3) and pyrrole C are observed[39] as in WT.

Structural perturbations could be expected for two residues that normally make contact with the native 2-vinyl (Phe138(H15)) and 4-vinyl (Ile99(FG5)) groups upon substitution by either hydrogen or acetyl groups. However, TOCSY and NOESY spectra reveal an Ile99(FG5) with a largely conserved orientation, with dipolar contacts to 3-CH_3 and 5-CH_3 in 2A,-4H-metMbCN (Figure 6A) and 2H,4A-metMbCN (Figure 6B), as observed[39] in WT, indicating inconsequential changes in orientation of these key residues. Similarly, the dipolar contacts between Phe138(H15) and 1-CH_3 are essentially unchanged in the two complexes relative to WT (not shown; see Supporting Information). Last, steady-state NOEs from the hemin 1-CH_3 and 8-CH_3 to the C_αH of Val68(E11) and $C_\beta H_3$ of Ala71(E14) are minimally perturbed[13,52] (not shown) in the two complexes relative to WT, indicating that the heme rotational position about the heme normal is not significantly altered by the modification of the positions 2- and 4-substituents. The chemical shifts for the hemin methyl and the His93(F8) proton peaks for the three complexes are listed in Tables 2 and 3, respectively.

For the other 2R,4R′-metMbCN complexes (except for R or R′ = F; see below), assignments due to isotope labeling at a

(50) Emerson, S. D.; Lecomte, J. T. J.; La Mar, G. N. *J. Am. Chem. Soc.* **1988**, *110*, 4176−4182.
(51) Qin, J.; La Mar, G. N. *J. Biomol. NMR* **1992**, *2*, 597−618.
(52) Rajarathnam, K.; Qin, J.; La Mar, G. N.; Chiu, M. L.; Sligar, S. G. *Biochemistry* **1993**, *32*, 5670−5680.

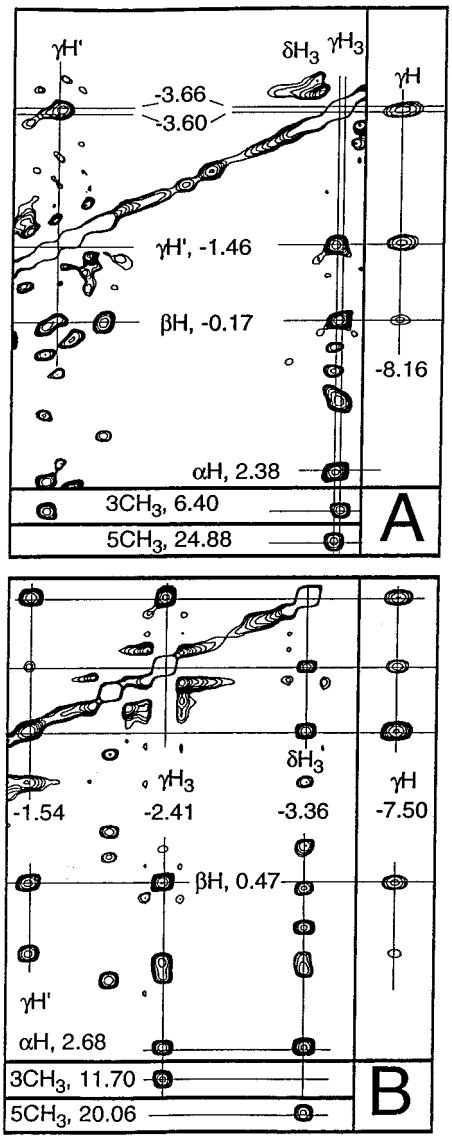

Figure 6. Portions of the 500-MHz ^{1}H NOESY spectra (τ_m = 100 ms) showing the largely conserved intraresidue and residue heme dipolar contacts for Ile99(FG5) in (A) 2H,4A-metMbCN at 20 °C and in (B) 2A,4H-metMbCN at 30 °C, both in ^2H_2O, 0.2 M NaCl, pH 8.6.

single position was sufficient to establish the orientation of the hemin in the pocket and provide, by analogy to WT, the methyl assignments presented in Table 1 (not shown; see Supporting Information). In limited cases, selective steady-state NOEs were determined[11] to confirm methyl assignments (not shown).

Magnetic Axes Determination for 2A,4H- and 2H,4A-MetMbCN. The magnetic axes,[20−22] α (direction of tilt of the major axis),[43] β (tilt from heme normal of major axis), $\kappa \sim \alpha + \gamma$ (location of rhombic axes;[43] see Figure 1) at 30 °C for each complex were determined by a three-parameter least-squares search using the WT anisotropies[22,48] ($\Delta\chi_{ax} = 2.58 \times 10^{-8}$ m^3/mol; $\Delta\chi_{rh} = -0.58 \times 10^{-8}$ m^3/mol) based on δ_{dip}(obs) for the protons on the structurally conserved assigned residues (identity and shifts given in Supporting Information). The resulting minimization yields[43] α = 145°, β = 14.3°, κ = −15° for 2A,4H− metMbCN, and α = 155°, β = 14.3°, κ = −15° for 2H,4A-metMbCN, which are very similar to each other and to the data on WT, α = 145°, β = 15.3°, κ = −15° using the same input data. The high quality of the fits is shown by the plot δ_{dip}(obs) vs δ_{dip}(calc) for the three complexes (Figure 7), as well as the low residual F/n (0.12 in all three cases).

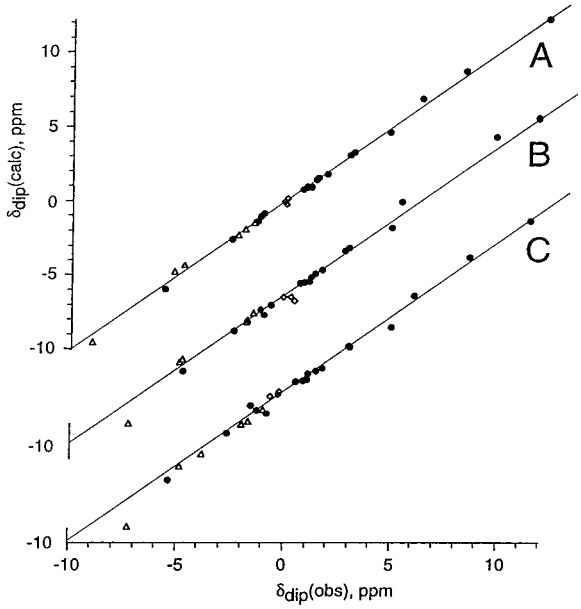

Figure 7. Plot of δ_{dip}(obs) versus δ_{dip}(calc) for the optimized magnetic axes from a three-parameter search for (A) wild-type metMbCN, (B) 2A,4H-metMbCN, and (C) 2H,4A-metMbCN using the same set as input data (solid circles). The data for Ile99(FG5) and Phe138(H15) not used in the fit are shown in open triangles and diamonds, respectively. The line of unit slope represents the perfect fit.

Knowledge of the magnetic axes allows calculation of δ_{dip} for the separation of the heme methyl and axial His protons, which, together with eqs 4 and 5, yield the contact shifts for the heme methyls and axial His in WT and the 2H,4A- and 2A,4H-metMbCN complexes, as shown in Table 2.

Temperature Dependence of Heme Methyl Shifts. The temperature dependence of the heme methyl shifts in 2A,4H-metMbCN and 2H,4A-metMbCN in a Curie plot (Figure 4B and D, respectively) reveals the presence of both positive (Curie-type) and negative (anti-Curie-type) slopes typical of cyanometglobins,[10−17] as well as other low-spin ferric hemoproteins.[18,19] The Curie slopes and apparent interecepts in Curie plots at T^{-1}= 0 for WT, 2H,4A- and 2A,4H-metMbCN are listed in Table 3.

Discussion

Qualitative Comparison among 2R,4R′-MetMbCN Complexes. It is noted that the strongly relaxed and two most strongly hyperfine shifted protons on nonligated residues in metMbCN,[39] the low-field C_ζH for Phe43(CD1), and the high-field C_γH for Ile99(FG5), exhibit essentially invariant hyperfine shifts of 17.0 ± 0.9 and −8.7 ± 0.9 ppm, respectively, as a function of 2R,4R′ (Table 1), including WT. Since these necessarily dipolar shifts for the nonligated residues reflect a combination of the magnetic anisotropy, the orientation of the principal magnetic axes, and the orientation of the Phe43(CD1) and Ile99(FG5) side chains relative to the iron center (geometric factors), as given in eq 2, the invariance of the shifts argues for conservation of all three properties for variable R,R′ in 2R,4R′-metMbCN complexes. This is confirmed in detail for 2H,4A- and 2A,4H-metMbCN above. Conversely, the highly variable contact shift dominated hemin methyl shift pattern with R,R′ (Table 1) attests to variable rhombic electronic asymmetry.

The peripheral substituents that lead to asymmetry[1,2] in the heme methyl contact shift of less than 20% (all combinations with R, R′ = M, E, V, H) also result in a conserved heme methyl contact shift pattern compared to WT metMbCN, with the 5-CH_3

Table 2. Separation of Dipolar and Contact Shifts for His93(F8) Protons in WT, 2H,4A- and 2A,4H-metMbCN[a]

		WT metMbCN				2H,4A-DH-metMbCN				2A,4H-DH-metMbCN			
proton	δ_{DSS}(dia)[b]	δ_{DSS}(obs)	δ_{hf}[c]	δ_{dip}[d]	δ_{con}[e]	δ_{DSS}(obs)	δ_{hf}	δ_{dip}	δ_{con}	δ_{DSS}(obs)	δ_{hf}	δ_{dip}	δ_{con}
$C_\alpha H$	2.9	7.4	4.5	4.5	0	7.8	4.9	5.1	−0.2	7.5	4.5	4.7	−0.2
$C_\beta H$	1.7	11.4	9.7	6.5	3.2	11.8	10.1	6.7	3.4	11.4	9.7	6.9	2.8
$C_\beta H'$	1.6	6.3	4.7	3.8	0.9	7.1	5.5	4.2	1.3	6.1	4.6	4.4	0.2
$C_\delta H$	1.1	−4.3	−5.4	−4.7	−0.7	0.0	−1.1	−2.1	1.0	−4.2	−5.3	−1.4	−4.0
$C_\epsilon H$	1.7	18.8	17.1	35.9	−18.8	22.6	20.9	34.6	−13.8	11.6	10.0	33.5	−23.4

[a] Shifts in ppm, at 30° in ^2H_2O, 0.2 M NaCl at pH 8.6. [b] In ppm referenced to DSS for MbCO.[44] [c] Obtained via eq 4. [d] Obtained via eq 2 for optimized magnetic axes. [e] Obtained via eq 5.

Table 3. Heme Methyl Shifts, Curie Slopes, and Curie Intercepts for 2H,4A-DH- and 2A,4H-MetMbCN[a]

	2H,4A-metMbCN			2A,4H-metMbCN		
	$\delta_{DSS(obs)}$	Curie[b] slope	Curie[c] intercept	δ_{DSS}(obs)	Curie slope	Curie intercept
1-CH_3	16.1	4.6	0	8.5	1.1	4
3-CH_3	3.9	−2.3	12	11.7	−1.0	15
5-CH_3	30.4	9.5	−2	20.1	5.6	3
8-CH_3	10.4	0.4	9	19.4	4.5	5

[a] Shift in ppm, referenced to DSS, in ^2H_2O, 0.2 M NaCl, pH 8.0 at 30 °C. [b] Slope in plot of d_{DSS}(obs) versus reciprocal absolute temperature, in ppm * K $\times 10^3$. [c] Intercept at $T^{-1} = 0$, in ppm, referenced to DSS.

> 1-CH_3 > 8-CH_3 > 3-CH_3 for the X-ray (Figure 1A) heme orientation, (i.e., the net peripheral electronic perturbations are smaller than the protein-induced rhombic perturbations). In the case of strong peripheral perturbation of the hemin by acetyl or formyl groups, the methyl contact shift pattern is strongly perturbed even outside the protein matrix,[28] with the electronic perturbation of the hemin comparable with that induced by the protein. Hence the methyl contact shift pattern in 2R,4R′-metMbCN with R or R′ = A or F can be significantly altered from that in WT. Heme methyl assignments were not pursued for 2F,4V-hemin (*spirographis*) and 2V,4F-hemin (*isospirographis*), either as model compounds or reconstituted into metMbCN. However, the very similar shifts in 2F,4V-hemin and 2A,4H-hemin, either as model or in Mb (and for both hemin orientations), and the similar shifts for 2V,4F-hemin and 2H-4A-hemin, either as model or in Mb (again for both hemin orientations), argue for the same assignments in the two complexes, with the effect of a combination formyl/vinyl group similar to that of an acetyl/hydrogen.

Modulation of the Hemin Rhombic Asymmetry in 2H,-4A- and 2A,4H-MetMbCN. These two hemins provide unique tests for the origin of the rhombic asymmetry because the direction of the electronic perturbations is known. Thus the electron-withdrawing 4-acetyl group (rhombic electronic perturbation approximately along the pyrrole II, IV vector) induces an in-plane asymmetry in the model compound that *generates a pattern of methyl contact shifts* similar to that imposed on an essentially 4-fold symmetric hemin upon incorporation into metMbCN in the orientation as found in WT Mb (Figure 1A). Not surprisingly, the additivity of the two similarly oriented perturbations leads to a conserved methyl contact shift pattern, but a significantly *enhanced spread* (∼27 ppm) *for the heme methyl shifts relative to WT* (Table 1), in the X-ray orientation (Figure 1A). In the same manner, the 2-acetyl group induces a similar rhombic perturbation approximately along the pyrrole I, III vector and results in a methyl contact shift pattern for the model complex *reversed* from that found in WT metMbCN (or as found[28,29] in metMbCN for the hemin orientation as in Figure 1B). Thus, upon incorporation of 2A,4H-hemin into the protein matrix in orientation A in Figure 1, the two rhombic perturbations are nearly orthogonal and tend to cancel, leading to 5-CH_3/8-CH_3 and 3-CH_3/1-CH_3 shifts that are pairwise very similar (Table 1) and to a strongly reduced methyl shift spread of only ∼10 ppm. It is noted that, as expected, 2A,4H-hemin leads to the larger heme methyl contact shift spread in the "reversed", or B heme orientation in metMbCN where the hemin electronic and protein-induced rhombic perturbations again add.

The simple model for the spread of the hemin methyl contact shift based on population of the alternate orbital states (Figure 2) dictates that, as the splitting between the d_{xz} and d_{yz} orbitals increases (decreases), the spread of the four heme methyl shifts increases (decreases), and the low-field methyl peaks (5-CH_3 and 1-CH_3) should show more positive (negative) slope and more negative (positive) apparent intercepts in a Curie plot. A quantitative analysis of the available data is not possible. On one hand, both dipolar and contact shifts contribute to δ_{hf}(obs), and, while δ_{dip} can be estimated with the magnetic axes, its temperature dependence is not expected to obey the simple Curie law with zero intercept.[9,22] On the other hand, the asymmetry in the methyl contact shifts of the model 2R,4R′-hemin$(CN)_2^-$ complexes must reflect a combination of perturbations of the coefficients of individual atoms in the molecular orbitals by the variable substituents, and the effect of lifting of the orbital degeneracy of d_{xz} and d_{yz}, which preferentially places the unpaired spin into one or another orbital. That the latter effect likely dominates is supported by the observations that for high-spin for iron(III) models[26,53,54] where each d orbital contains one spin, the asymmetry in the heme methyl contact shift is considerably smaller than in the low-spin, biscyano complexes.[2,26,54] Moreover, the biscyano complexes of 2H,4A-hemin and 2A,4H-hemin, with rhombic perturbation on a single pyrrole, exhibit the expected pairs of low-field methyls with hyper-Curie, and high-field methyls with hypo-Curie behavior for the hyperfine shifts (Figure 4A, C), as observed in WT metMbCN.[10,11] Therefore we ignore for the present the smaller dipolar shift and any significant change in the nature of the π MOs.

Comparison of the hemin methyl shifts, slopes, and intercepts in the metMbCN complexes in Table 2 and Figure 4B and D shows that, indeed, the methyl shifts spread is *larger*, slopes *more positive*, and apparent intercepts *more negative*, for 1-CH_3 and 5-CH_3 in 2H,4A-metMbCN than in 2A,4H-metMbCN. On the other hand, the 3-CH_3, 8-CH_3, slopes are *more negative* and the apparent intercept,[56] for at least 3-CH_3, is *more positive* in 2H,4A-metMbCN than in 2A,4H-metMbCN. Thus, the difference in the heme methyl shift patterns between the two

(53) Budd, D. L.; La Mar, G. N.; Langry, K. C.; Smith, K. M.; Nayyir-Mazhir, R. *J. Am. Chem. Soc.* **1979**, *101*, 6091−6096.
(54) La Mar, G. N.; Walker, F. A. In *The Porphyrins*; Dolphin, D., Ed.; Academic Press: New York, 1978; pp 61−157.
(55) Satterlee, J. D.; La Mar, G. N. *J. Am. Chem. Soc.* **1976**, *98*, 2804−2808.
(56) Miki, K.; Harada, S.; Hato, Y.; Iba, S.; Kai, Y.; Kasai, N.; Katsube, Y.; Kawabe, K.; Yoshida, Z.; Ogoshi, H. *J. Biochem.* **1986**, *100*, 277−284.

complexes can be qualitatively rationalized by simply a larger rhombic splitting in 2H,4A-metMbCN, where the substituent and protein effects add, than in 2A,4A-metMbCN, where they largely cancel. Since 2H,4A-hemin$(CN)_2^-$ exhibits essentially the same methyl contact shift pattern, with the same characteristic temperature behavior, as a "symmetric" heme in metMbCN, it is reasonable to conclude that the 4-acetyl group and the axial His bond raise the d_{xz}, d_{yz} orbital degeneracy by comparable amounts. However, since a vinyl group is much less electron withdrawing than an acetyl group, it is expected that a vinyl group would contribute less to the splitting. At the present, it is not possible to guage directly the influence of a vinyl group because the available hemins all have a non-methyl substituent at both the 2- and 4-positions, and all but methyl and ethyl groups have a marked effect on the electron asymmetry in even the model compound.[1,2] A more quantitative estimate of the influence of a single substituent would be to use hemin where 2R = alkyl and 4R = V, A, H or 2R = V, A, H and 4R = alkyl; such studies are in progress.

The analyses of 2A,4H-metMbCN and 2H,4A-metMbCN demonstrate that the peripheral substitution of the hemin can significantly affect the rhombic splitting of d_{xz} and d_{yz} orbitals in a predictable manner because the appropriate orientation of both the substituent and protein-induced perturbations are known. A converse to this is that the rhombic asymmetry in a given low-spin ferrihemoprotein reflects *both the electronic effect of substituents and the orientation of the axial His imidazole(s)* and that the orbital hole does not necessarily uniquely indicate the orientation of the axial His in a *b*-type hemoprotein. In fact, instead of a heme contact shift pattern serving as a quantitative indicator for the orientation of an axial His, the combination of the contact shift pattern and the crystallographically determined axial His orientation should ultimately identify the exact nature of other protein-induced rhombic perturbations.

Modulation of Axial His Hyperfine Shifts in 2H,4A- and 2A,4H-MetMbCN. The His93(F8) protons exhibit both δ_{con} and δ_{dip}, of which the latter can be calculated on the basis of the magnetic axes determined[20,22] above for these two complexes (eqs 2, 4, and 5). The resulting δ_{hf}, δ_{dip}, and δ_{con} for the two subject complexes, and those for WT, are compared in Table 2. The results are consistent with previous analyses of the hyperfine shifts in low-spin ferrihemin models[54,55] and ferrihemoproteins[19,20,22] in that primarily $C_\epsilon H$ of the axial His exhibits significant π contact shifts. Comparison of the His93-(F8) shifts in 2A,4H-metMbCN and 2H,4A-metMbCN with those in WT (Table 2) reveals that mainly $C_\epsilon H$ exhibits a significant shift difference, which, upon factoring into δ_{dip} and δ_{con}, shows that the $C_\epsilon H$ contact shift is *smaller* by ~5 ppm in 2A,4H-metMbCN, and *larger* by ~5 ppm in 2H,4A-metMbCN than WT metMbCN. On the basis of an orbital hole determined primarily by the axial His, large π contact shifts are *allowed only in the ground-state* d_{yz} orbital hole and not in the excited-state d_{xz} orbital hole.[6] This leads to the expectation that an increased (decreased) splitting between the ground- and excited-state orbital states should lead to increased (decreased) π contact shifts for the axial His, as observed. Hence, the pattern of axial His shift changes parallels the heme methyl shift changes predicted by the simple model depicted in Figure 2.

Empirical Interpretation of Heme Methyl Shifts in 2R,-4R′-MetMbCN. We emphasize here the effects of the protein matrix in modifying the individual methyl shifts of a hemin upon incorporation into metMbCN. The influence on individual methyl groups of the hemin upon incorporation into the protein matrix is provided by 2M,4M-hemin. Comparison of the ^1H NMR spectra for the essentially 4-fold symmetric 2M,4M-hemin-$(CN)_2^-$ with that for 2M,4M-metMbCN reveals[11] that the six individual methyl groups experience chemical shift changes Δ(i-CH_3), $i = 1-5$, eight methyls, due to their local environment, as given by

$$\Delta(\text{i-CH}_3) = \delta^{\text{i}}[\text{2M,4M-metMbCN} - \text{2M,4M-hemin(CN)}]_2^- \quad (6)$$

which yields Δ(1-CH_3) = +5.3, Δ(2-CH_3) = +2.8, Δ(3-CH_3) = −9.9, Δ(4-CH_3) = −6.8, Δ(5-CH_3) = 8.1, and Δ(8-CH_3) = −4.8 ppm. If we assume that the protein exerts a similar "rhombic" effect, Δ(i-CH_3), for methyl i on each hemin in the X-ray orientation (Figure 1A), we obtain a "predicted" heme methyl shift, δ_{DSS}(pred) pattern for all other hemins via eq 7:

$$\delta^{\text{i}}_{\text{DSS}}[\text{pred for 2R,4R-metMbCN}] = \delta^{\text{i}}_{\text{DSS}}[\text{obs for (2R,4R′-hemin(CN)}_2^-] + \Delta(\text{i-CH}_3) \quad (7)$$

It is noted that the "addition" of the effects of the hemin substituents (shifts in the model) and the protein influence can predict the hemin methyl shift patterns for *the reversed heme orientation* (Figure 1B) by simply recognizing that in the 180° rotated heme interchange the 1 ↔ 4, 2 ↔ 3, and 5 ↔ 8 positions (i.e., the 1-CH_3 (and 3-CH_3) experience the "protein" influence reflected in the 4-CH_3 (and 2-CH_3) of 2M,4M- metMbCN, etc.). The predicted shifts for each of the hemins in each of the two orientations in 2R,4R-metMbCN are given in parentheses in Table 1. A plot of δ_{DSS}(obs) versus δ_{DSS}(pred) (via eqs 6 and 7) is shown in Figure 8; an excellent correlation is observed for all but two methyls on the strongly rhombically perturbed hemin.

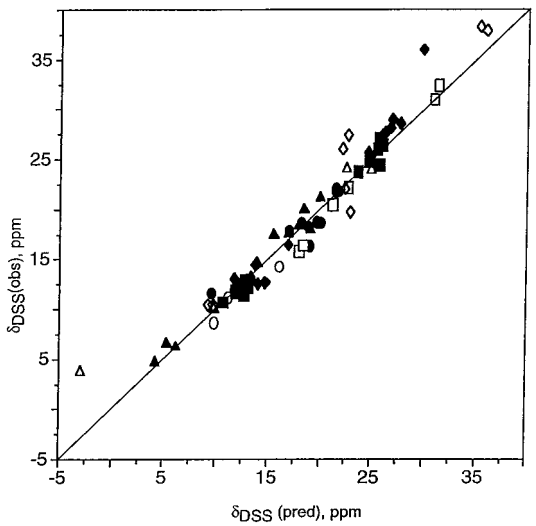

Figure 8. Plot of δ_{obs}^{i}(2R,4R′-metMbCN) versus δ_{DSS}^{i}(pred for 2R,4R′-metMbCN) for methyls i = 1, 3, 5, and 8 for all complexes listed in Table 1, with the latter determined via eqs 6 and 7. The data for the rhombical weakly to moderately perturbed hemins (2R,4R ≠ A or F) are shown in filled markers, while data for strongly rhombically perturbed hemins (2R and/or 4R = A or F) are shown by open markers. The heme positions are marked by circles (1-CH_3), triangles (3-CH_3), squares (5-CH_3) and diamonds (8-CH_3).

Practical implications of the empirical correlation between the hemin methyl shifts as a model compound and in metMbCN is that assignment of hemin methyls peaks of a peripherally functionalized hemin cyanoferrihemoprotein and in the extracted

model compound should shed light on the relative orientation of the heme and the axial His in the protein. Conversely, highly perturbed methyl contact shift patterns in a cyanoferrihemoprotein with an axial His could be used to deduce the nature and/or location of peripheral functional groups on the heme.

Heme Orientational Preferences. Following to equilibrium the methyl peak intensities for the two 2R,4R′-metMbCN complexes generated immediately after reconstitution, together with either 1D/2D NMR or isotope labeling,[28−30,35] yields the equilibrium constants for formation of the complex with the heme orientation 180° rotated about the α,γ-meso axis relative to WT Mb. The data in Table 1 show that, in all cases but one (2H,4E-hemin), the major isomer is that with the crystallographic heme orientation (Figure 1A), with the $K_{eq} = 0.02-0.1$ for the hemins investigated. For 2H,4E-metMbCN, the bulky 4-ethyl group destabilizes the crystallograph heme orientation (A in Figure 1) by >1.6 kcal/mol relative to the other hemins. In fact, the "reversed" or heme orientation B in Figure 1B is the *dominant* species in solution at ambient temperatures for 2H,4E-metMbCN. It is clear that the protein more readily accommodates large substituents at its 2- than at its 4-position. The present results on hemin orientation are qualitatively consistent with previous crystallographic studies[56] of 2H,4V-, 2V,4H-, 2H,4E-, and 2E,4H-metMbH_2O in identifying the predominant hemin orientation. However, in the crystal structures, only one orientation was detected, even for 2H,4E-Mb, which exhibits a ∼1:2 ratio of the isomers in solution.

Acknowledgment. The authors are indebted to Dr. Z. Xia for providing Figure 2 and for valuable discussions. This research was supported by grants from the National Institutes of Health, HL16087 (G.N.L.) and HL22252 (K.M.S.).

Supporting Information Available: Six figures (^{1}H NMR spectra of 2A,4A-, 2V,4F-, 2F,4V-, 2H,4V-, 2V,4H-, 2H,4E- and 2E,4H-metMbCN and portions of NOESY maps for 2A,-4H- and 2H,4A-metMbCN, and three tables (chemical shifts for 2R,4R′-hemin(CN_2^-); chemical shifts for heme and heme pocket residues in 2H,4A-metMbCN and 2A,4H-metMbCN). See any current masthead page for ordering information and Web access instructions.

JA983045X